VACUUM AND CRYOGENIC (3 K TO 675 K) PROBE STATIONS:

A Versatile Tool for Materials and Device Characterization

JANIS

Probe station cooling options

Liquid helium (LHe) or nitrogen (LN_2)

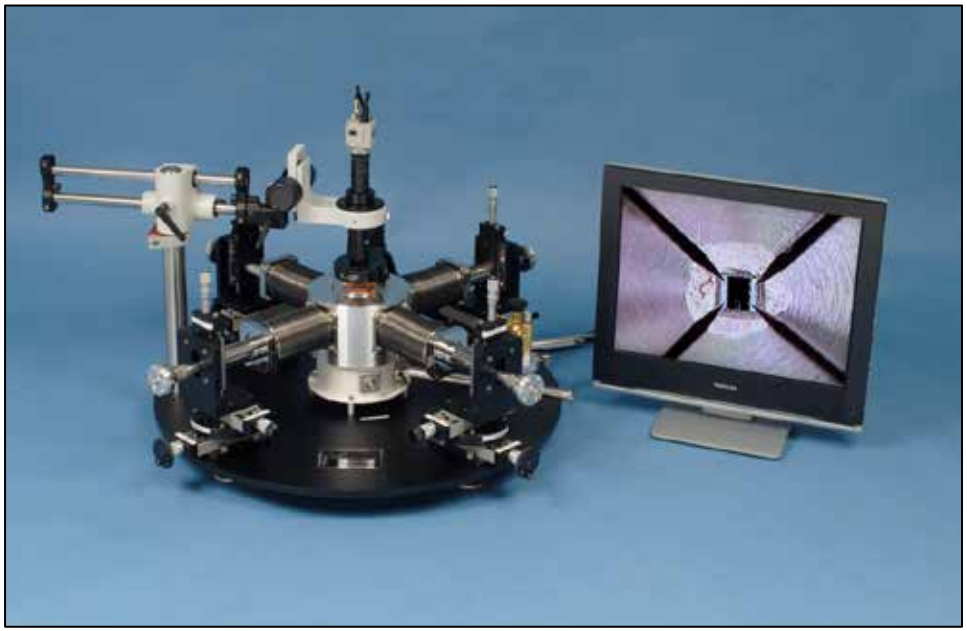

Cryogenic refrigerator

Cryogenic Refrigerator

- Recirculating helium gas provides cooling. No LHe or LN_2 is required.
- Includes a compressor (air- or water-cooled), flexible metal supply and return gas lines, and refrigerator (cold head).
- Base temperatures ranging from <4 K to 10 K.
- Janis works with world leaders in cryocooler technology, including Sumitomo Heavy Industries (SHI) and Brooks Automation (CTI).

More Probe Station Options

Ultra High Vacuum
Cryogenic & Room temperature
Large sample size (200 mm)

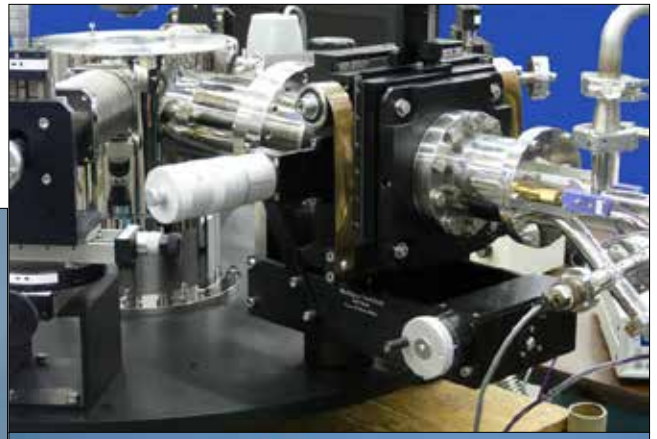

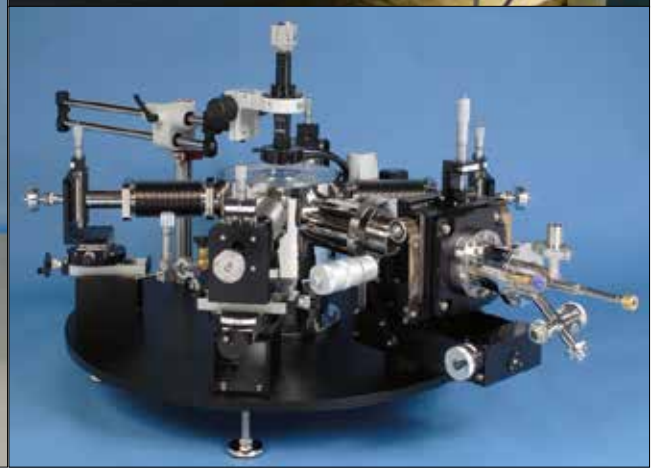

Electrical Probes
Low Frequency (DC)

Janis probe stations use standard commercially available probe tips

Tips are easily removed and exchanged

Tip materials include tungsten, beryllium copper, nickel, gold plated

Tip point radius from 0.1 microns to 200 microns

Tip configurations include low contact resistance, bendable, cat whisker, and others

Low thermal contraction probe arms substantially reduce thermal drift of the probe tip

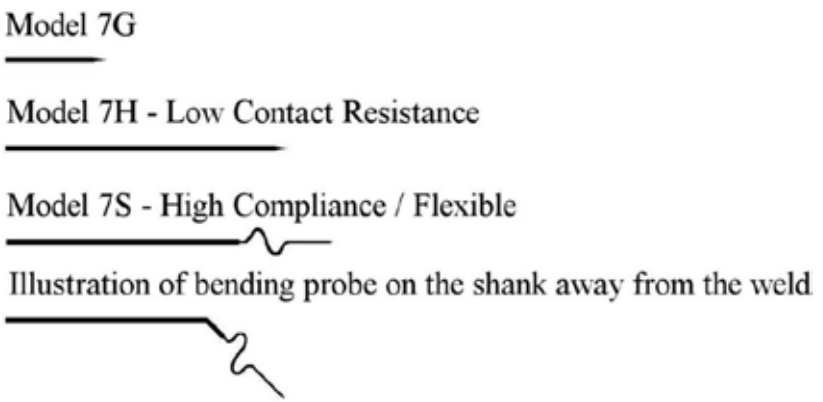

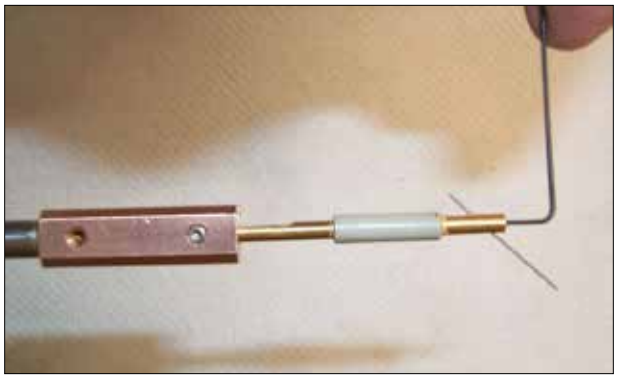

Electrical Probes
Low Frequency (DC)

General purpose
BNC or SMA
Coaxial cable

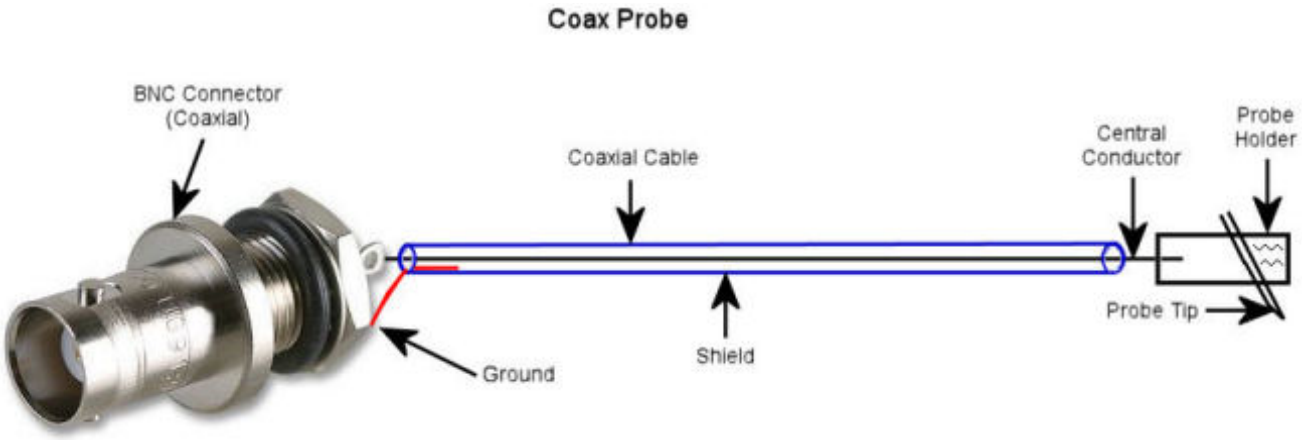

Low current
Triaxial connector
Triaxial cable
Includes “guard”

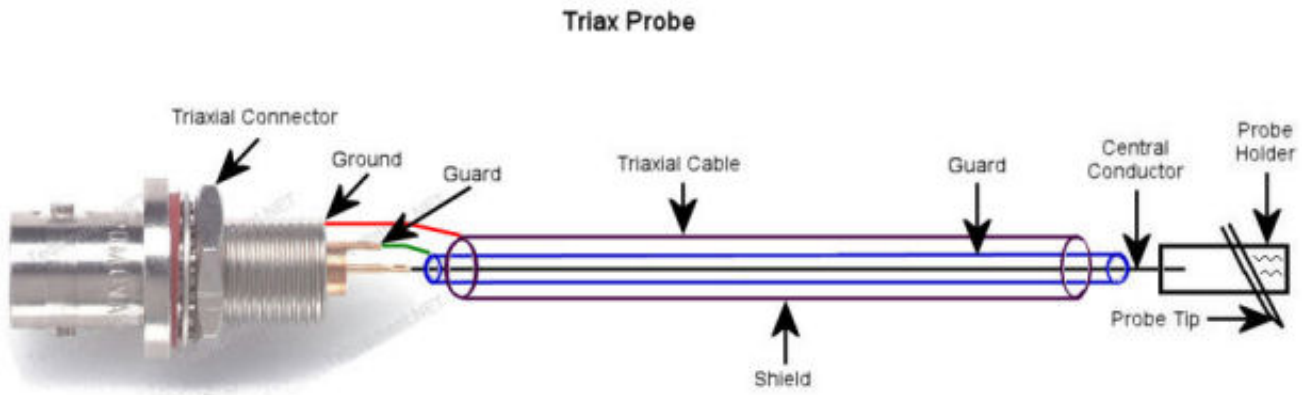

Electrical Probes
High Frequency (MW)

40, 50, and 67 GHz frequency
GSG (most common), GS, and SG
Each probe is wired with semi-rigid coaxial cable
K-connector, 2.4 mm connector, or V-connector
Probe arms include theta-rotation for planarization

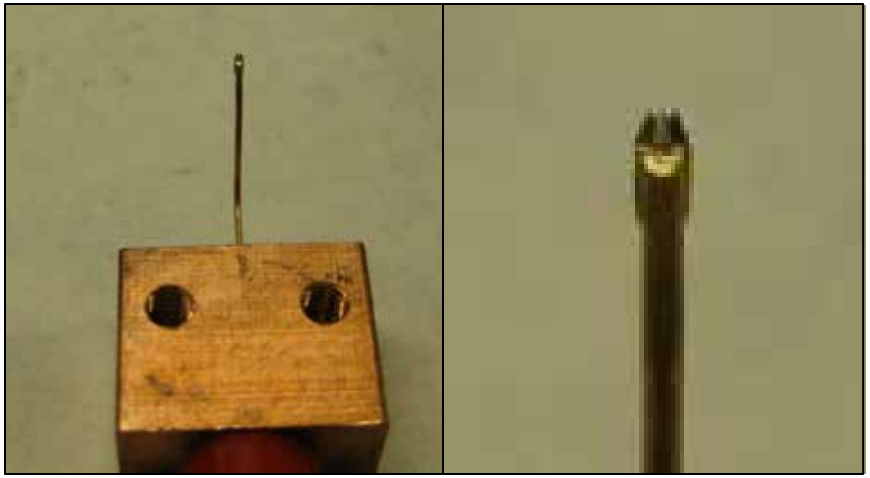

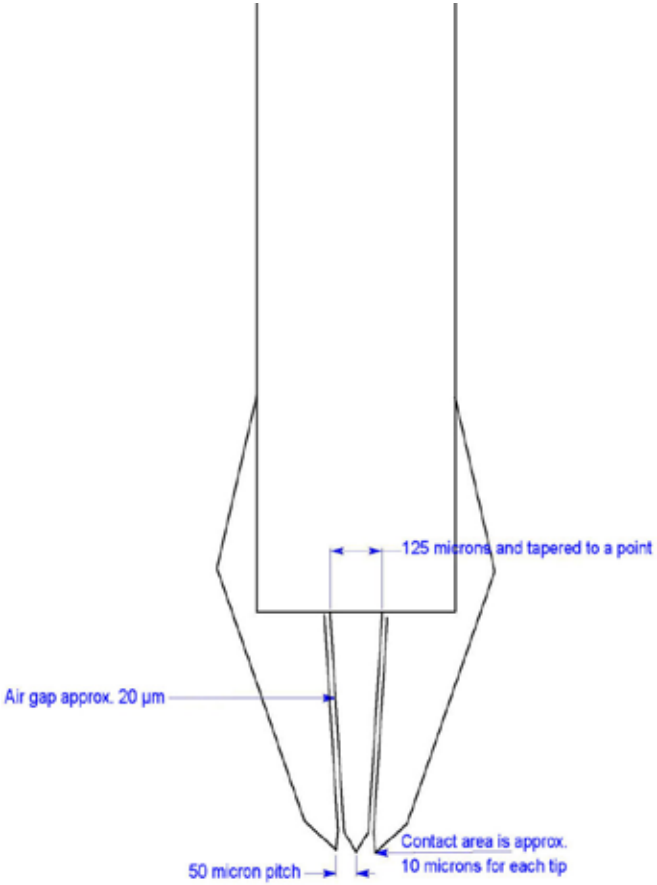

Magnetic Options

Electromagnet

Superconducting magnet

Permanent magnet

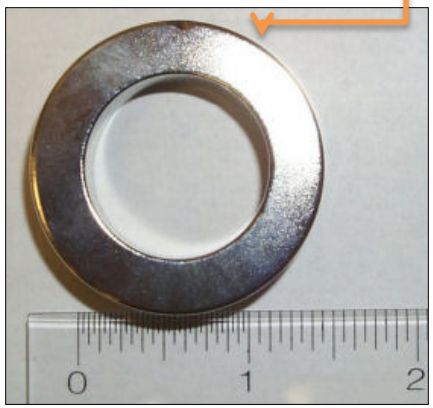

Optics

Monoscope
Optical resolution 5, 3.4, 2.2 micrometer
CCD/USB camera, output to monitor or PC

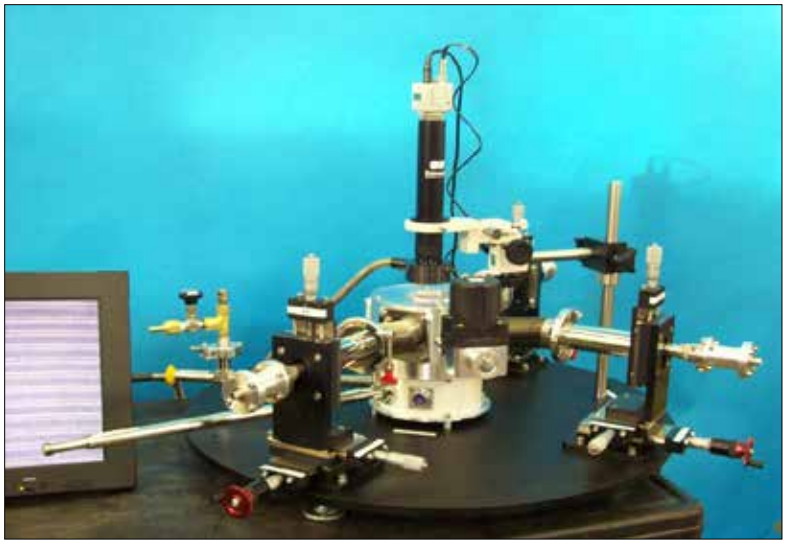

Fiber optic probe arm
Single or multimode, UV, VIS-NIR
SMA or FC connector

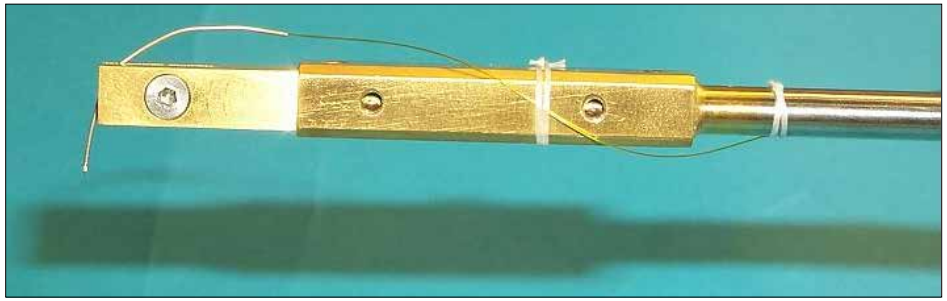

MOSFETS – Conventional Transistor

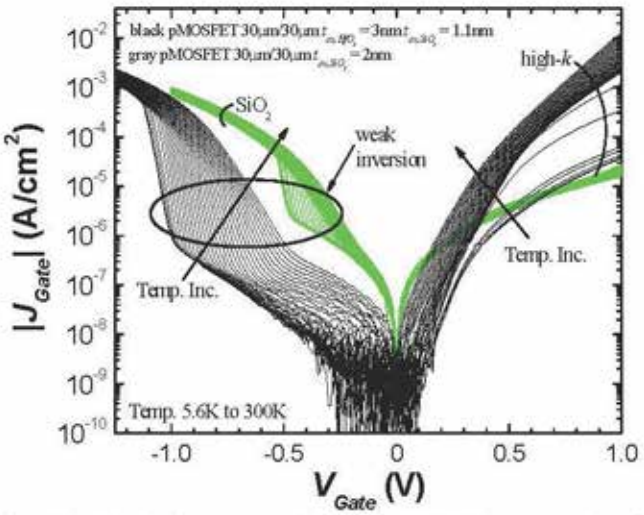

Fig. 3: Gate leakage current for pMOSFETs composed of a HfO_2/SiO_2 gate dielectric and a SiO_2 gate dielectric for temperatures ranging from 5.6K to 300K. The encircled region marks the weak inversion regime. For accumulation (positive voltages), the gate leakage current decreases dramatically at very low temperatures ~25K.

Source: Professor William Knowlton, Materials Science & Engineering | Electrical & Computer Engineering, Boise State University

Reference: Richard Southwick III*, J. Reed*, C. Buu*, H. Bui*, R. Butler*, G. Bersuker, and W.B. Knowlton, **Temperature (5.6-300K) Dependence Comparison of Carrier Transport Mechanisms in HfO_2/SiO_2 and SiO_2 MOS Gate Stacks**, paper presentation at the 2008 IEEE International Integrated Reliability Workshop, (October 12-16, 2008), p.48-54. Invited to submit an extended version of this paper to IEEE Transactions on Materials and Device Reliability. http://dx.doi.org/10.1109/IRWS.2008.4796084

Organic Electronics

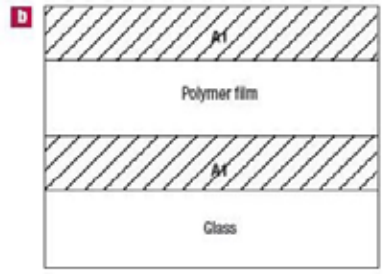

Figure 1 Current–voltage curve (b) for a device of structure Al/Au–DT+8HQ+PS/Al. A, B and C in a represent the first, second and third bias scans, respectively. The arrows in a indicate the voltage-scanning direction.

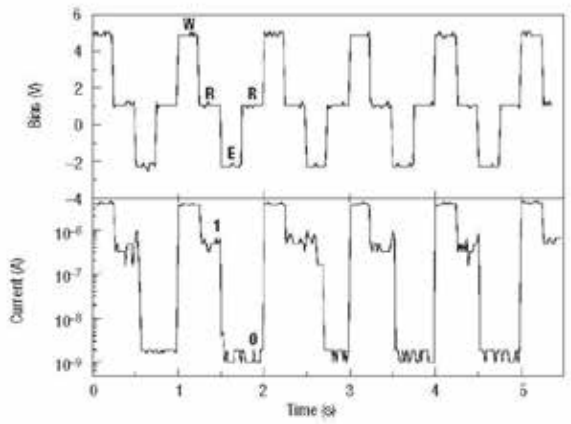

Figure 2 Write–read–erase cycles of device Al/Au–DT+8HQ+PS/Al. The top and bottom curves are the applied voltage and the corresponding current response, respectively. W, R and E in the top figure mean write, read and erase, respectively. The labels '1' and '0' in the bottom figure indicate the device in the high- and low-conductivity state, respectively.

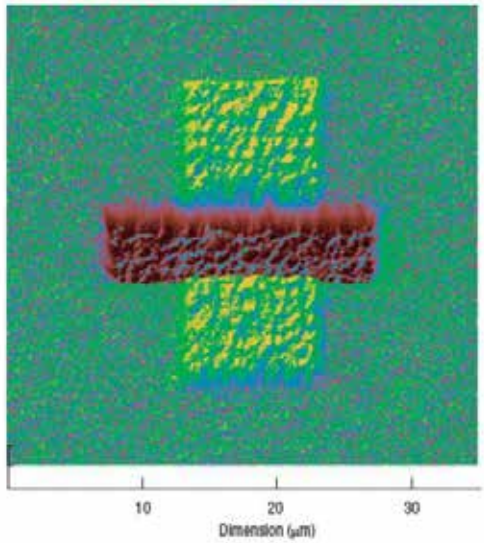

Figure 5 Scanning surface potential AFM image of Au–DT+8HQ+PS film with aluminium as bottom electrode and silicon wafer as substrate. The vertical bar (yellow) was pre-treated with a +10-V d.c. bias, and the horizontal bar (brown) was pre-treated with a −10-V d.c. bias.

Source: Professor Yang Yang, University of California, Los Angeles, Department of Materials Science & Engineering. http://yylab.seas.ucla.edu/index.aspx

Reference: Jianyong Ouyang, Chih-Wei Chu, Charles R. Szmanda, Liping Ma, Yang Yang, "Programmable polymer thin film and non-volatile memory device," *Nature Materials, 3, 12, December (2004)* http://www.ncbi.nlm.nih.gov/pubmed/15568028

Organic Electronics

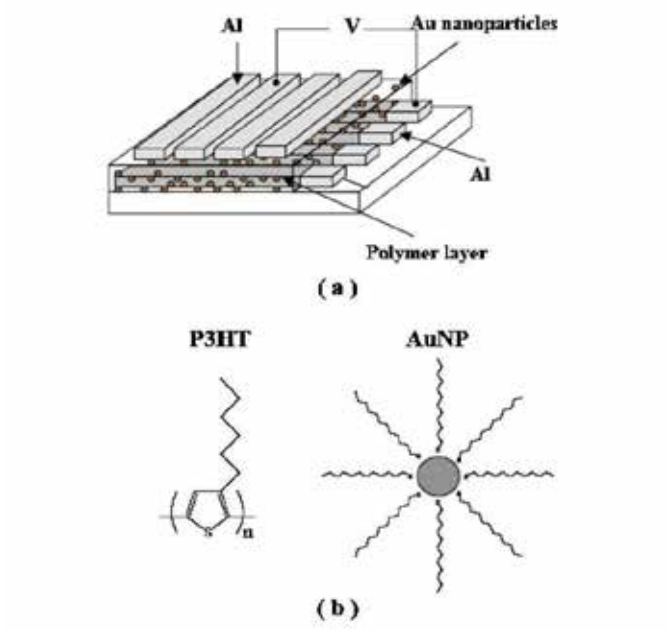

FIG. 1. (Color online) (a) Device structure and (b) chemical structures of P3HT and the Au NP.

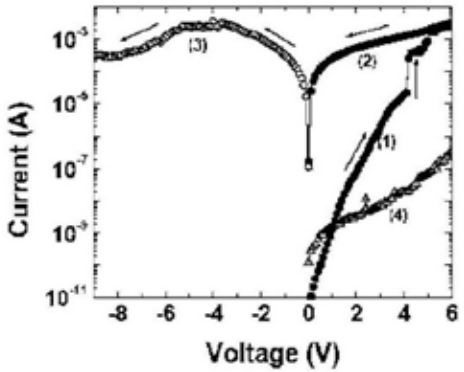

FIG. 2. Current-voltage (*I-V*) curves for the Al/Au NPs+P3HT/Al and Al/P3HT/Al devices. Curves (1), (2), and (3) represent the first, second, and third bias scans of the former device, with the arrows indicating the direction of the scans, and curve (4) is the *I-V* curve of the latter device.

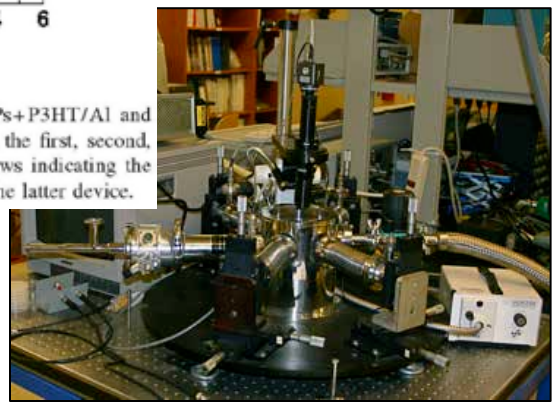

Source: Professor Yang Yang, University of California, Los Angeles, Department of Materials Science & Engineering. http://yylab.seas.ucla.edu/index.aspx

Ankita Prakash, Jianyong Ouyang, Jen-Lien Lin, Yang Yang, "Polymer memory device based on conjugated polymer and gold nanoparticles," *Journal of Applied Physics, 100, 054309 (2006)* http://dx.doi.org/10.1063/1.2337252

Organic Electronics

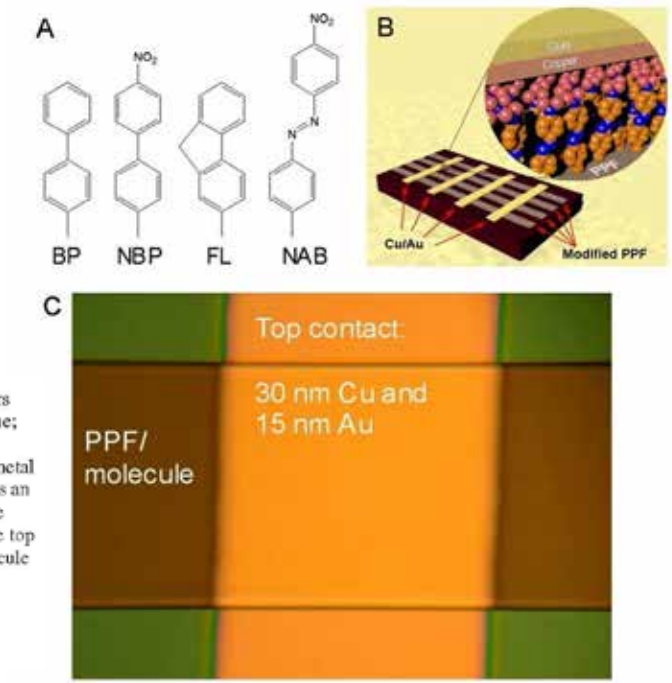

Figure 1. (A) Molecular structures and abbreviations for adlayers used in this study (BP, biphenyl; NBP, nitrobiphenyl; FL, fluorene; NAB, nitroazobenzene). (B) Schematic representation of carbon–molecule–copper junction where each point at which a metal stripe crosses the PPF is a single junction. The inset in (B) shows an idealized molecular level depiction of the layered structure of the cross-junction. (C) Micrograph of an actual junction showing the top contact stripe oriented vertically across the horizontal PPF/molecule strip. The bias voltage is applied by contacting micromanipulator-controlled probes on the PPF and top contact immediately adjacent to the junction.

(This figure is in colour only in the electronic version)

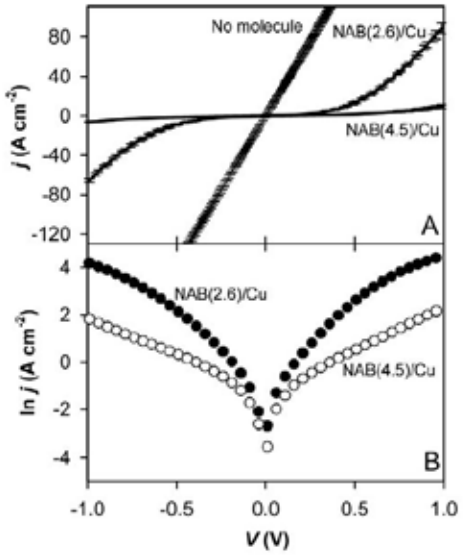

Figure 2. (A) j–V curves for three junctions: PPF/Cu, PPF/NAB(2.6)/Cu, and PPF/NAB(4.5)/Cu. The error bars represent ±one standard deviation for three to five junctions. (B) ln j versus V plot for the molecule-containing junctions. Sweep rate 10^3 V s^{-1}, geometric junction areas 5×10^{-4} cm^2.

Source: Dr. Richard L. McCreery, National Institute for Nanotechnology, University of Alberta, Canada

Reference: Adam Bergren, Kenneth Harris, Fengjun Deng, and R. L. McCreery, "Molecular Electronics using Diazonium-Derived Adlayers on Carbon with Cu Top Contacts: Critical Analysis of Metal Oxides and Filaments", *J. Phys. Cond. Mat.* 2008, 20, 374117. (invited) http://iopscience.iop.org/0953-8984/20/37/374117/

Organic Electronics - Ratchets

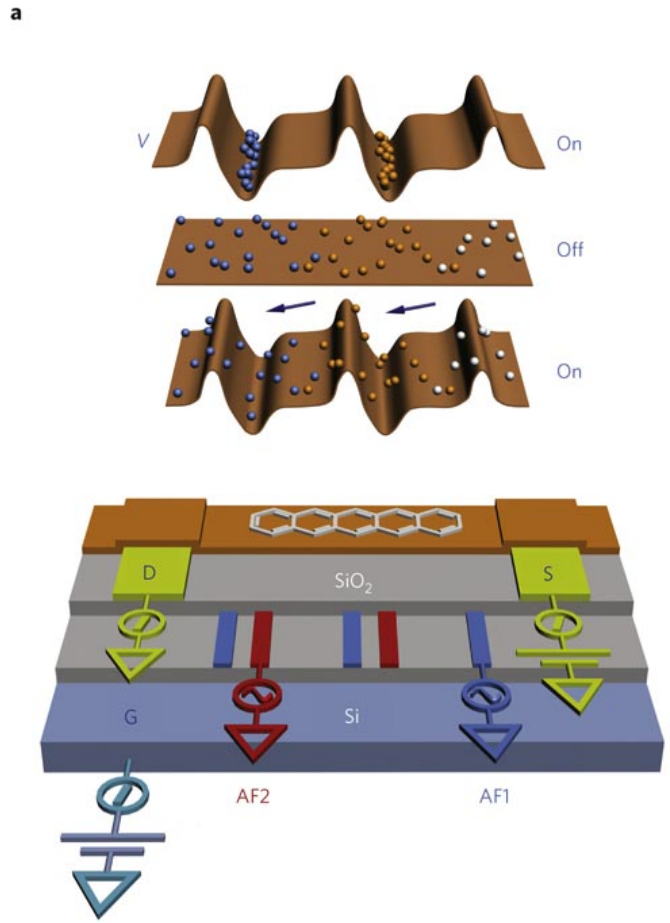

Figure 1 | Ratchet mechanism and proof of principle. a, Schematic representation of the flashing ratchet mechanism with a schematic drawing of an investigated ratchet. Visible are the source (S) and drain (D) contacts, which are separated from the silicon (Si) gate (G) contact by the silicon dioxide (SiO_2) gate dielectric. Asymmetrically spaced interdigitated finger electrodes denoted by AF1 and AF2 are placed inside the gate dielectric. Note the colour coding of the finger electrodes; fingers with the same colour are electrically connected. The device is covered with pentacene, represented by the orange layer.

Source: Dr. Wijnand Germs, Applied Physics, University of Technology Eindhoven, The Netherlands

Reference: Erik M. Roeling, Wijnand Chr. Germs, Barry Smalbrugge, Erik Jan Geluk, Tjibbe de Vries, René A. J. Janssen & Martijn Kemerink, "Organic electronic ratchets doing work," *Nature Materials,* **10**, 51–55 (2011) doi:10.1038/nmat2922

www.nature.com/nmat/journal/v10/n1/full/nmat2922.html

Quantum Dots

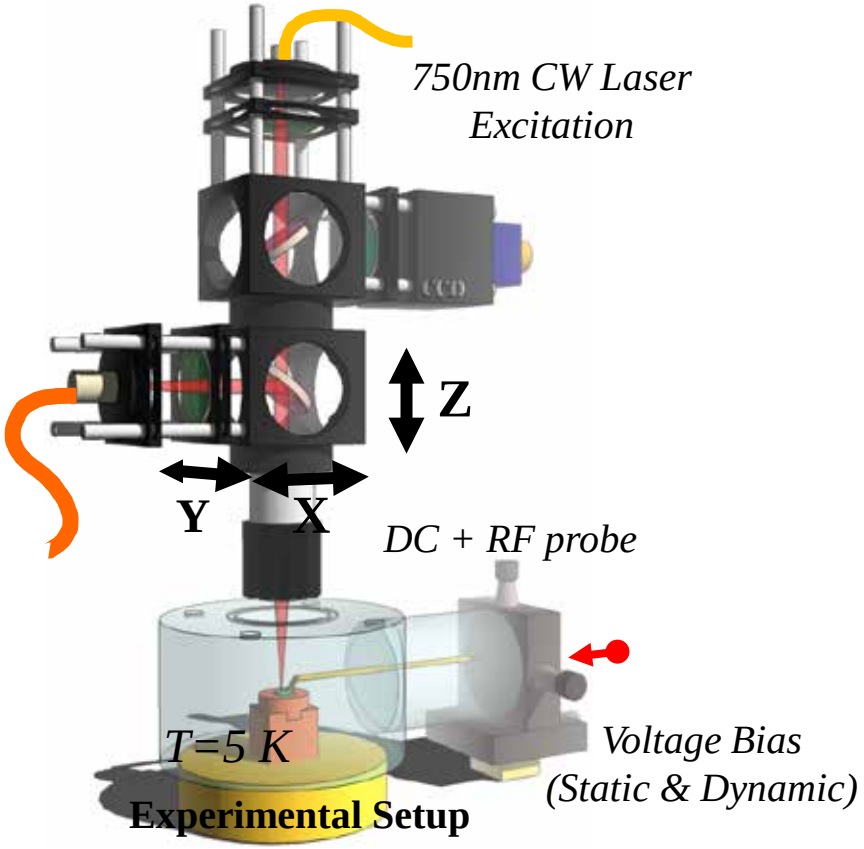

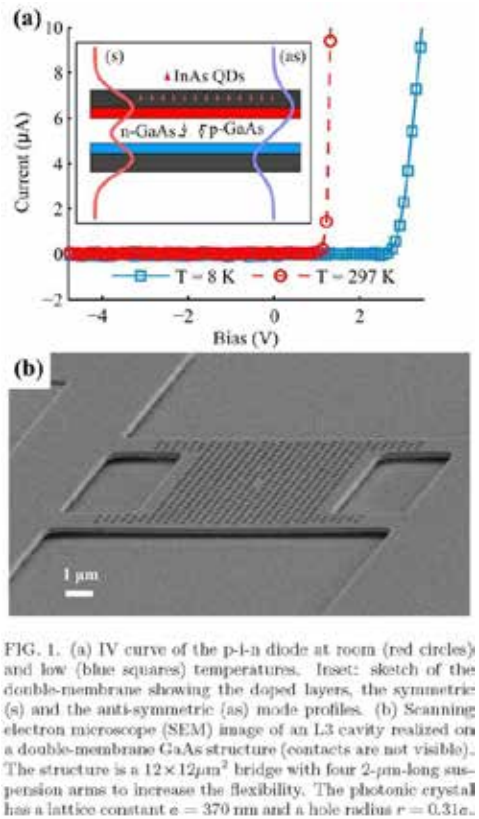

FIG. 1. (a) IV curve of the p-i-n diode at room (red circles) and low (blue squares) temperatures. Inset: sketch of the double-membrane showing the doped layers, the symmetric (s) and the anti-symmetric (as) mode profiles. (b) Scanning electron microscope (SEM) image of an L3 cavity realized on a double-membrane GaAs structure (contacts are not visible). The structure is a $12\times12\mu m^2$ bridge with four 2-μm-long suspension arms to increase the flexibility. The photonic crystal has a lattice constant $a = 370$ nm and a hole radius $r = 0.31a$.

Source: Francesco Pagliano and Andrea Fiore, Photonics and Semiconductor Nanophysics Group, Dep. Applied Physics, Eindhoven University of Technology, contact person Prof. A. Fiore. Reference: Midolo et al., arxiv:1207.2980 (2012)
http://arxiv.org/abs/1207.2980

Quantum Dots

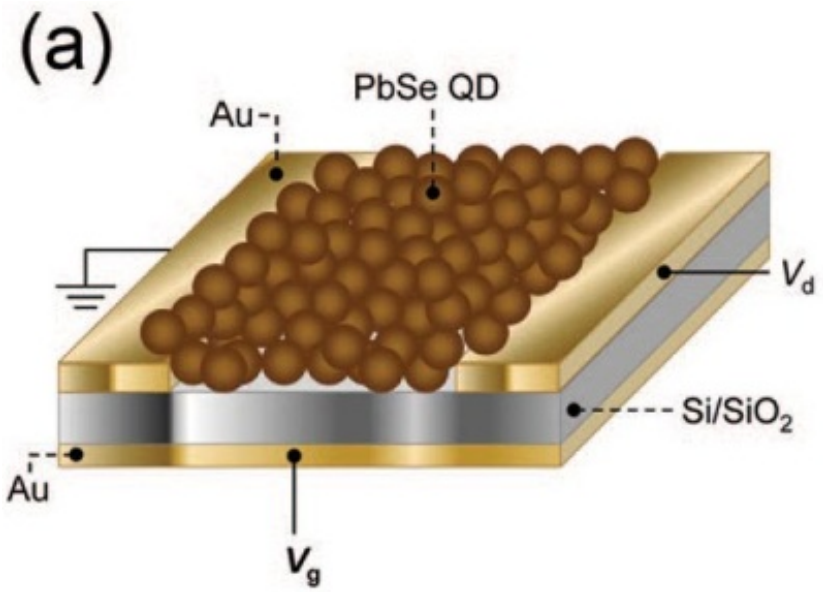

Figure 1. (a) Schematic of the back-gated PbSe QD FET (not to scale).

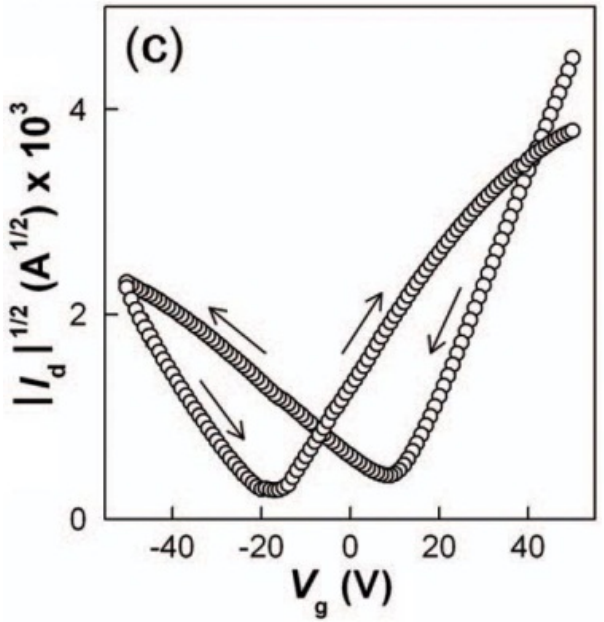

Figure 3. (c) Draincurrent-gate-voltage (*I*d-*V*g) plots (or transfer characteristics) of an EDT-treated PbSe QD FET recorded at *V*d) -40 V under vacuum and in the dark.

Source: Professor Eray Aydil, University of Minnesota

Reference: Kurtis S. Leschkies, Moon Sung Kang, Eray S. Aydil and David J. Norris, "Influence of Atmospheric Gases on the Electrical Properties of PbSe Quantum-Dot Films," *J. Phys. Chem. C*, **2010**, *114* (21), pp 9988–9996
http://pubs.acs.org/doi/abs/10.1021/jp101695s

Solar Cells

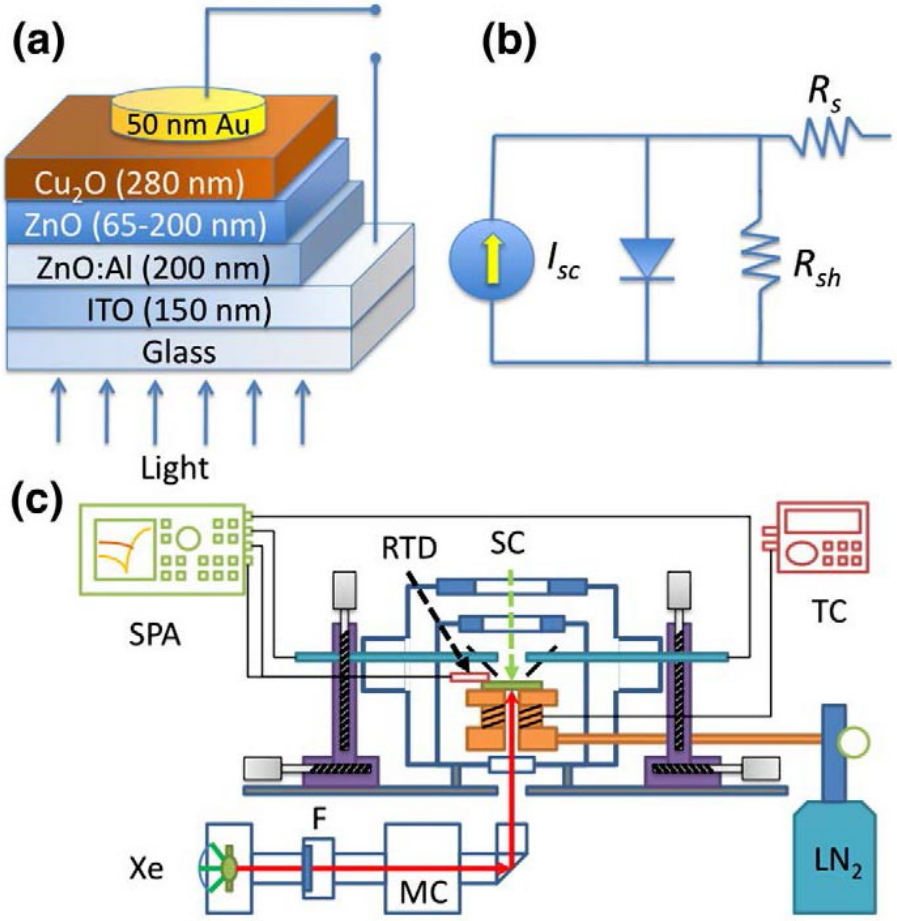

Fig. 1. (a) Schematic of the Cu2O/ZnO heterojunction solar cell. In some cells a 10 nm thick TiO2 layer was also inserted between the ZnO and Cu2O layers. (b) A schematic of a common equivalent circuit for the solar cell in (a). (c) Schematic of the micromanipulated cryogenic cryomicroprobe station with illumination capabilities used for the J–V–T measurements. F: filters; MC: monochromator; RTD: resistance temperature detector; SC: solar cell; SPA: semiconductor parameter analyzer; TC: temperature controller; Xe: Xe arc lamp.

Source: Professor Eray Aydil, University of Minnesota

Reference: SeongHo Jeong, Sang Ho Song, Kushagra Nagaich, Stephen A. Campbell, Eray S. Aydil, "An analysis of temperature dependent current–voltage characteristics of Cu_2O–ZnO heterojunction solar cells," *Thin Solid Films*, Thin Solid Films 519, 6613-6619 (2011). http://dx.doi.org/10.1016/j.tsf.2011.04.241

Solar Cells

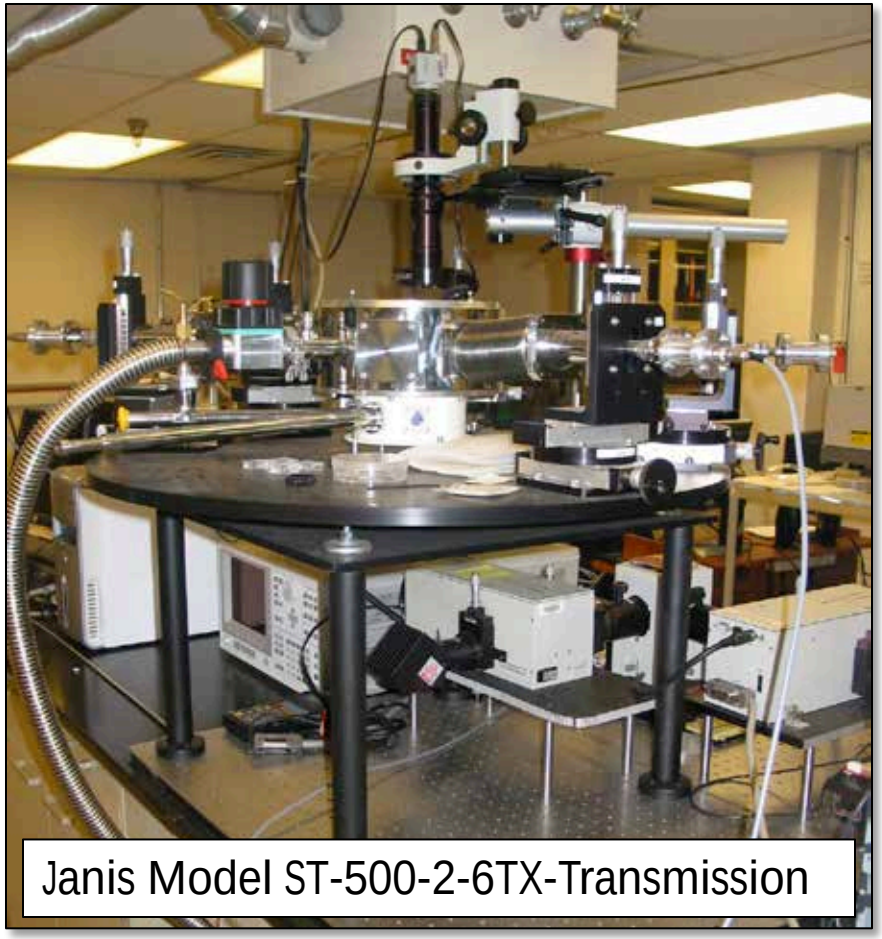

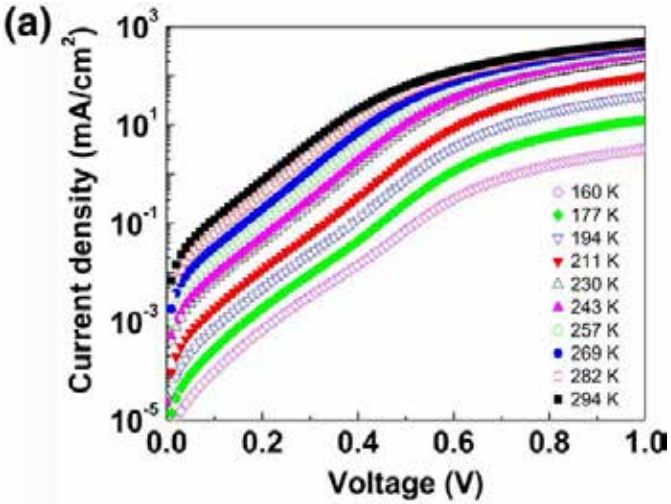

Fig. 2. Dark *J-V* characteristics of Cu_2O/ZnO solar cells as a function of temperature between 160 K and 295 K. The thin film stack that comprised this solar cell was Au/Cu_2O/ZnO/AZO/ITO/Glass: (a) 65 nm thick ZnO.

Source: Professor Eray Aydil, University of Minnesota

Reference: SeongHo Jeong, Sang Ho Song, Kushagra Nagaich, Stephen A. Campbell, Eray S. Aydil, "An analysis of temperature dependent current–voltage characteristics of Cu_2O–ZnO heterojunction solar cells," *Thin Solid Films*, Thin Solid Films 519, 6613-6619 (2011). http://dx.doi.org/10.1016/j.tsf.2011.04.241

MEMS – Square Plate Resonators

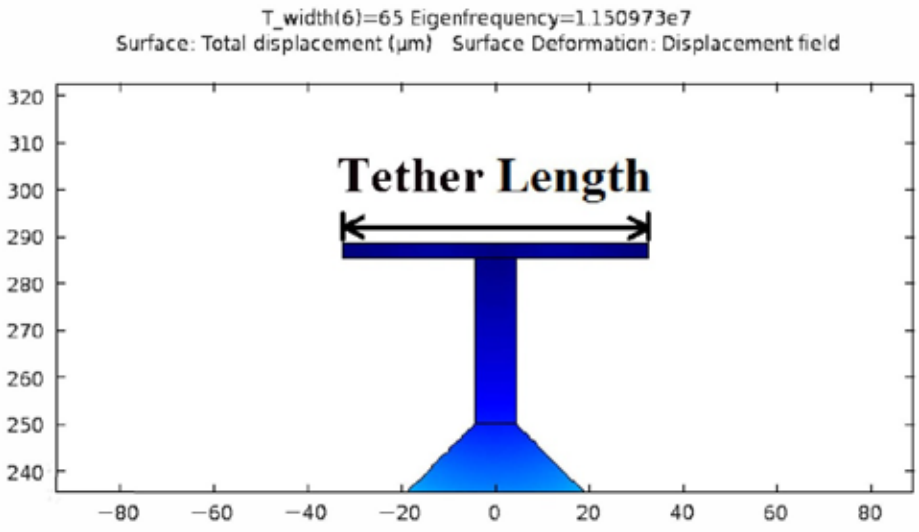

Fig. 3. Definition of the T-shaped tether length.

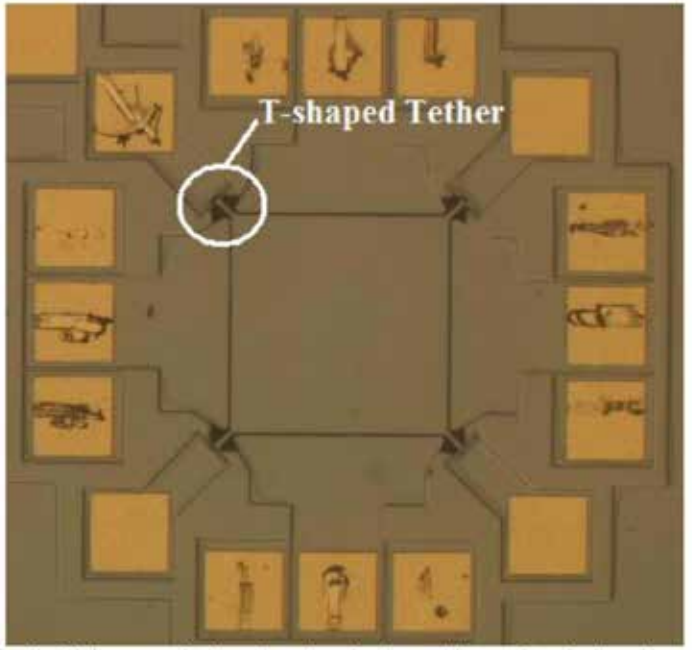

Fig. 4. Micrograph showing the device with standard tether length

Source: Professor Joshua Lee, Department of Electronic Engineering, City University of Hong Kong: www.ee.cityu.edu.hk/~joshulee

Reference: Y. Xu and J. E.-Y. Lee, "Evidence on the impact of T-shaped tether variations on Q factor of bulk-mode square-plate resonator," in Proceedings of the 7th IEEE International Conference on Nano/Micro Engineered and Molecular Systems (IEEE NEMS 2012), Kyoto, Japan, 5-8 Mar 2012, pp. 463-468. http://dx.doi.org/10.1109/NEMS.2012.6196818

MEMS – Square Plate Resonators

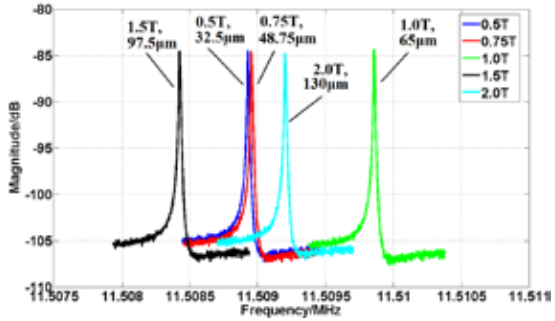

Measured Transmission

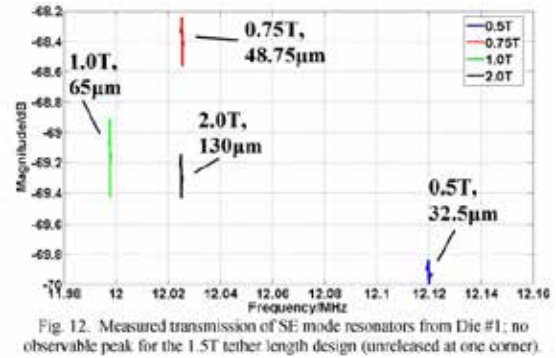

Fig. 12. Measured transmission of SE mode resonators from Die #1; no observable peak for the 1.5T tether length design (unreleased at one corner).

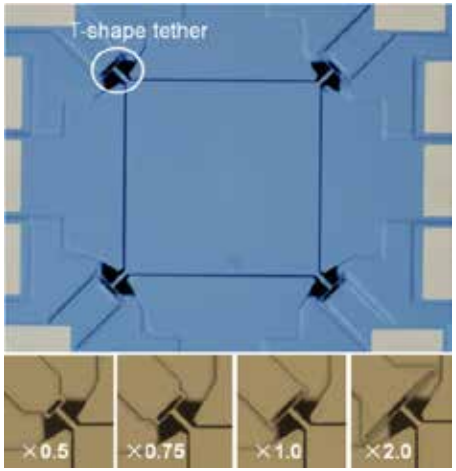

Micrograph of the Resonator and a Corner Tether from each of the 5 Resonators

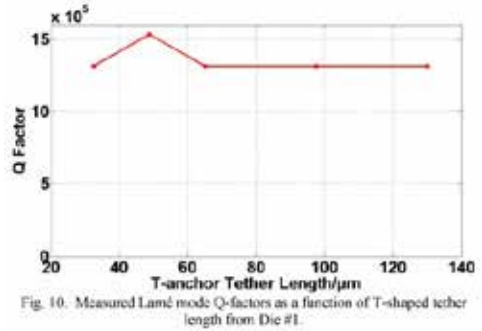

Fig. 10. Measured Lamé mode Q-factors as a function of T-shaped tether length from Die #1.

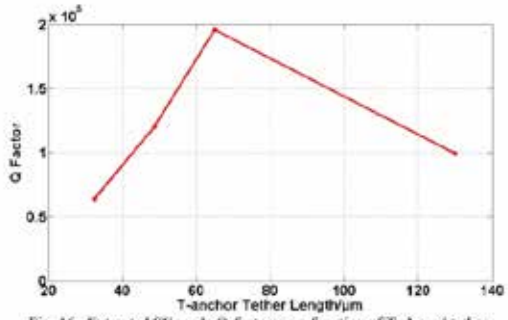

Fig. 16. Extracted SE mode Q-factors as a function of T-shaped tether length measured from Die #1.

Source: Professor Joshua Lee, Department of Electronic Engineering, City University of Hong Kong: www.ee.cityu.edu.hk/~joshulee

Reference: Y. Xu and J. E.-Y. Lee, "Evidence on the impact of T-shaped tether variations on Q factor of bulk-mode square-plate resonator," in Proceedings of the 7th IEEE International Conference on Nano/Micro Engineered and Molecular Systems (IEEE NEMS 2012), Kyoto, Japan, 5-8 Mar 2012, pp. 463-468. http://dx.doi.org/10.1109/NEMS.2012.6196818

Carbon Nanotubes

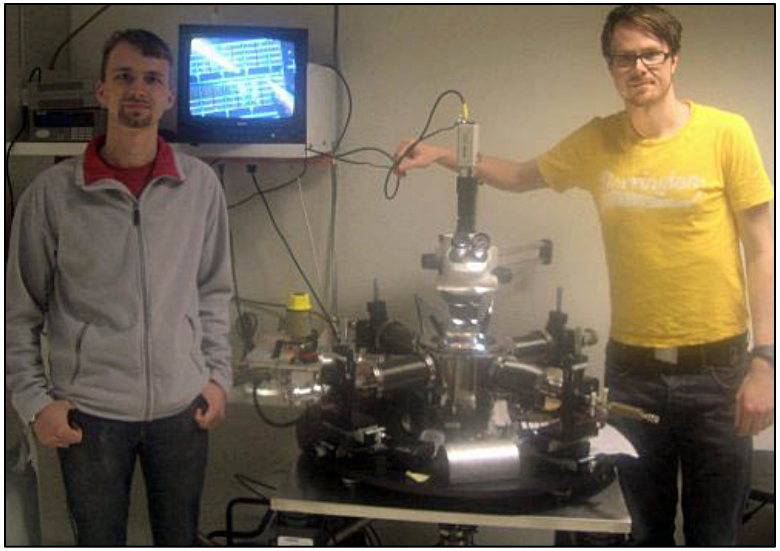

Johannes Svensson and Yury Tarakanov with the cryogenic probe station.

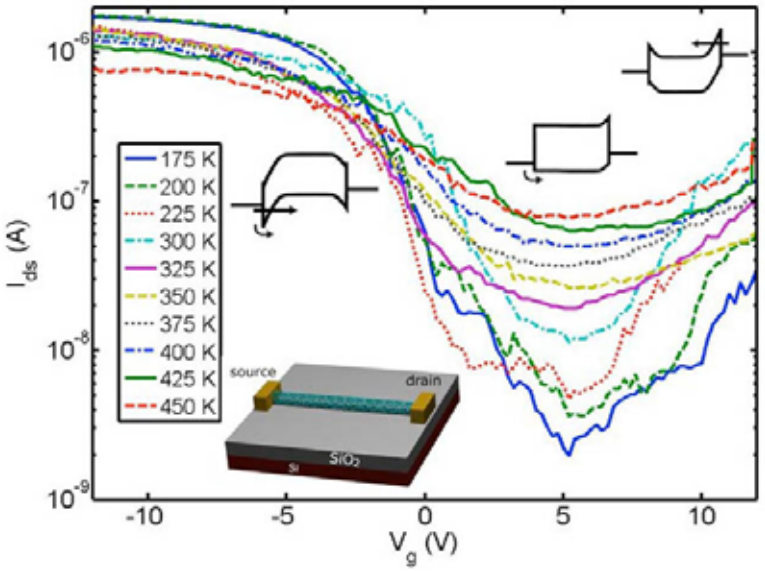

Characterizing a carbon nanotube transistor: current as a function of gate voltage measured at different temperatures.

Source: Professor Eleanor Campbell and Dr. Johannes Svensson, formerly of Gothenburg University, Sweden and currently at Edinburgh University, UK and Lund University, Sweden respectively.

Reference: Svensson J, Sourab AA, Tarakanov Y, Lee DS, Park SJ, Baek SJ, Park YW, Campbell EE, "The dependence of the Schottky barrier height on carbon nanotube diameter for Pd-carbon nanotube contacts.;" Nanotechnology. 2009 Apr 29;20(17):175204. http://www.ncbi.nlm.nih.gov/pubmed/19420588 and http://nanotechweb.org/cws/article/tech/39382.

Graphene

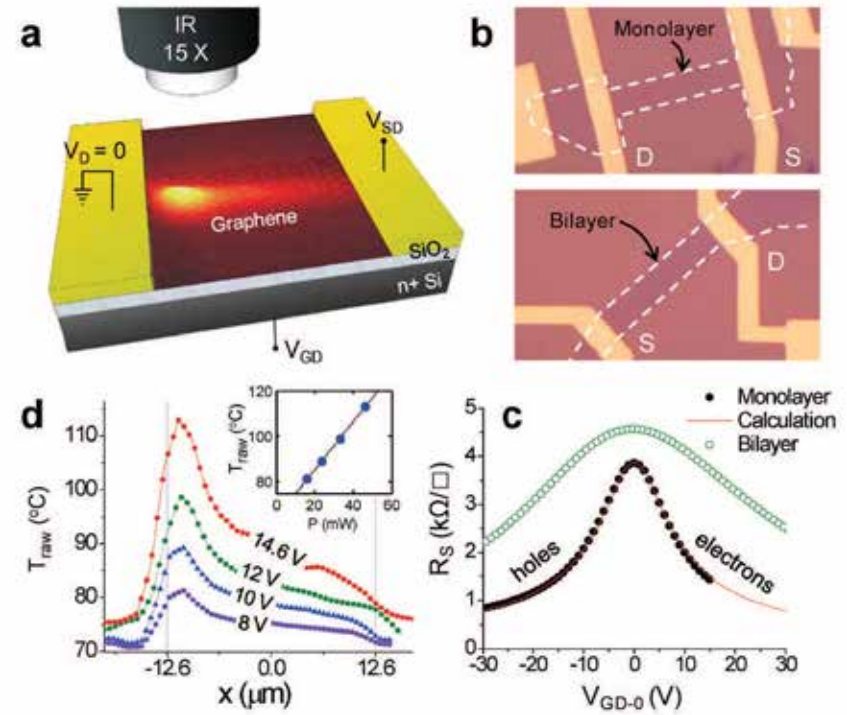

FIGURE 1. Graphene field effect transistors (GFETs). (a) Schematic of GFET and infrared (IR) measurement setup.11 Rectangular graphene sheet on SiO2 is connected to metal source (S) and drain (D) electrodes. Emitted IR radiation is imaged by 15x objective. (b) Optical images of monolayer (25.2 × 6 μm2) and bilayer (28 × 6 μm2) GFETs. Dashed lines indicate graphene contour. (c) Sheet resistance vs back-gate voltage *V*GD-0) *V*GD - *V*0 (centered around Dirac voltage *V*0) of monolayer (closed points) and bilayer GFETs (open points) at *T*0) 70 °C and ambient pressure. (d) Imaged (raw) temperature along middle of monolayer GFET at varying *V*SD and *V*GD-0) -33 V (hole-doped regime). Dotted vertical lines indicate electrode edges. The inset shows linear scaling of peak temperature with total power input. Temperature rise here is raw imaged data (*T*raw) rather than actual graphene temperature.

Source: Professor Eric Pop, Electrical and Computer Engineering, University of Illinois at Urbana-Champaign

Reference: M.-H. Bae, Z.-Y. Ong, D. Estrada, E. Pop, "Imaging, Simulation, and Electrostatic Control of Power Dissipation in Graphene Devices," *Nano Letters* **10**, 4787, (2010). **Selected as cover article of *Nano Letters*, December 2010**
http://dx.doi.org/10.1021/nl1011596

Graphene

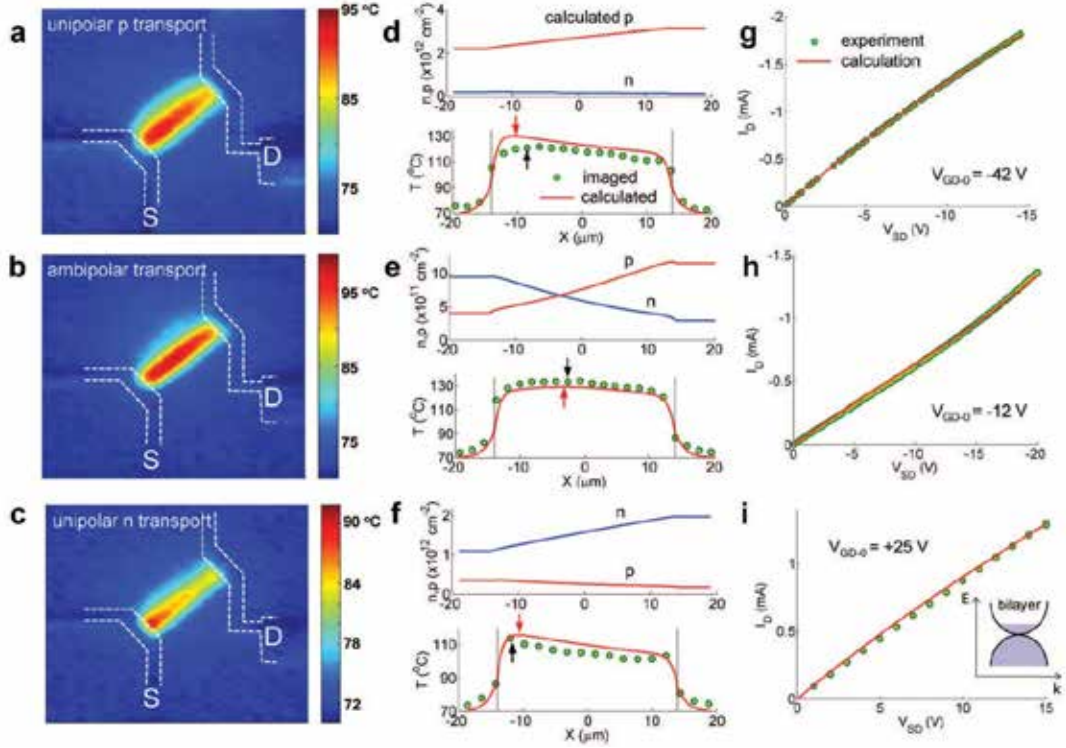

FIGURE 3. Electrostatics of bilayer GFET hot spot. Imaged temperature map of bilayer GFET for: (a) *V*GD-0) -42, (b) -12, and (c) 25 V with corresponding *V*SD)-14.5, -20, and 15 V, respectively. (d-f) Electron and hole density (upper panels, simulation) and temperature profiles (lower panels). Symbols are experimental data and solid lines are calculations. Arrows indicate calculated (red) and experimental (black) hot spot positions, in excellent agreement with each other, and with the position of lowest charge density, as predicted by simulations. (g-i) Corresponding *I-V* curves (symbols are experiment and solid lines are calculations). Temperature maps were taken at the last bias point of the *I-V* sweep. The temperature profile of the bilayer GFET is much broader than that of the monolayer (Figure 2), a direct consequence of the difference in the band structure and density of states (Figures 2i and 3i insets).

Source: Professor Eric Pop, Electrical and Computer Engineering, University of Illinois at Urbana-Champaign

Reference: M.-H. Bae, Z.-Y. Ong, D. Estrada, E. Pop, "Imaging, Simulation, and Electrostatic Control of Power Dissipation in Graphene Devices," *Nano Letters* **10**, 4787, (2010). **Selected as cover article of *Nano Letters*, December 2010.**
http://dx.doi.org/10.1021/nl1011596

Graphene Oxide

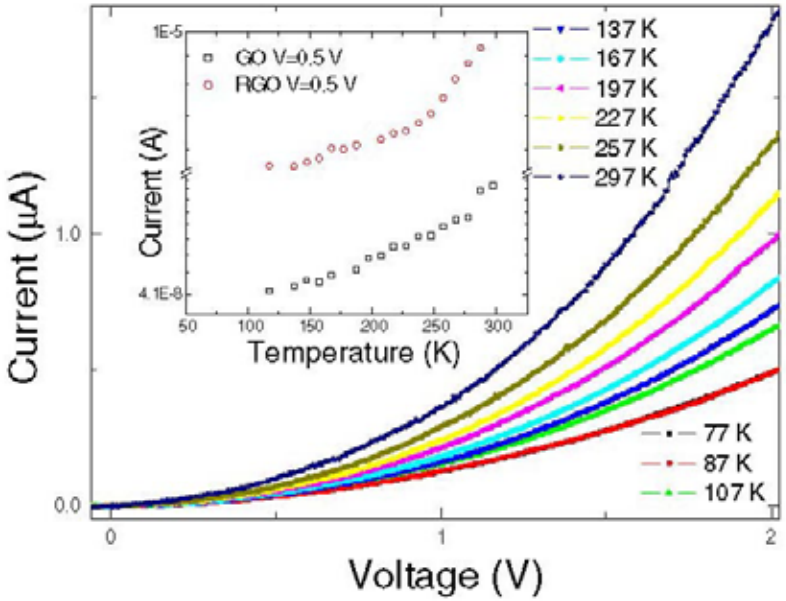

Fig. 1: (Colour on-line) I-V measurements for GO. Inset: current as a function of temperature for GO and RGO.

Source: Professor Somnath Bhattacharyya , Nano-Scale Transport Physics Laboratory, School of Physics, University of the Witwatersrand, Johannesburg, South Africa

Reference: Ross McIntosh, Messai A. Mamo, Brice Jamieson, Saibal Roy and Somnath Bhattacharyya, "Improved electronic and magnetic properties of reduced graphene oxide films," 2012 *EPL* **97** 38001, http://dx.doi.org/10.1209/0295-5075/97/38001

Superconducting Photon Detector

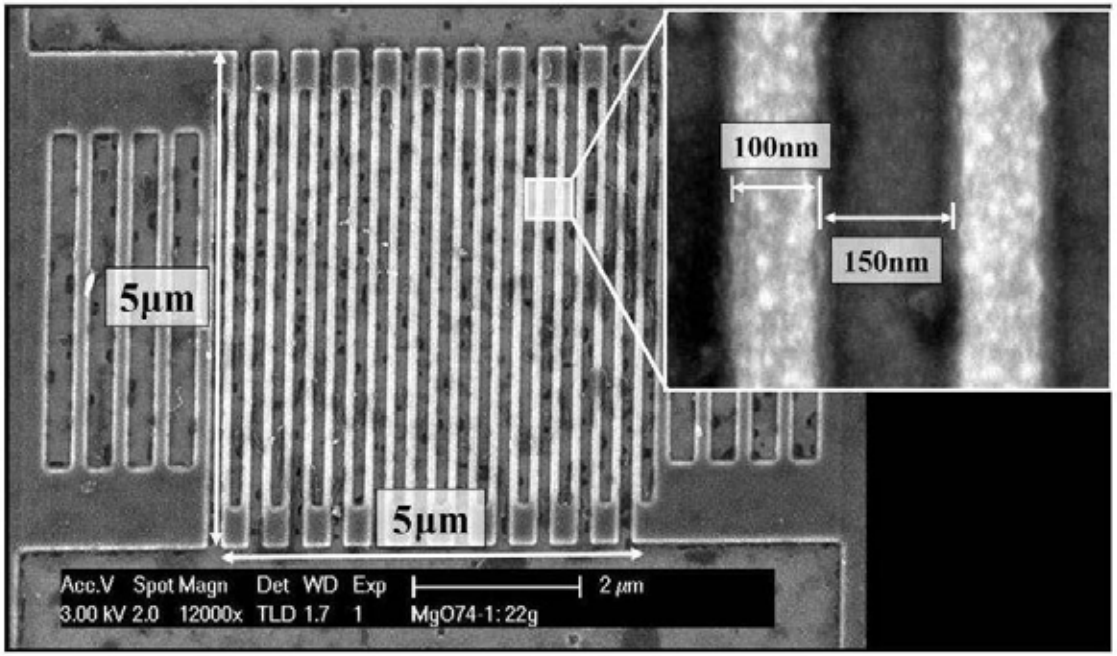

Fig. 2. Scanning electron microscope (SEM) image of an SSPD. The nanowire width is w=100nm, the fill factor is f =40%. The inset shows an ultra-high resolution image of two stripes. The mean width variation was estimated to be Δw ~10nm.

Source: Professor Francis Lévy, EPFL, Switzerland and Prof. Andrea Fiore, Photonics and Semiconductor Nanophysics Group, Dep. Applied Physics, Eindhoven University of Technology, contact person Prof. A. Fiore.

Reference: F. Marsili, D. Bitauld, A. Fiore, A. Gaggero, F. Mattioli, R. Leoni, M. Benkahoul, and F. Lévy**,** "High efficiency NbN nanowire superconducting single photon detectors fabricated on MgO substrates from a low temperature process," Optics Express, Vol. 16, Issue 5, pp. 3191-3196 (**2008**)
http://dx.doi.org/10.1364/OE.16.003191

Superconducting Photon Detector

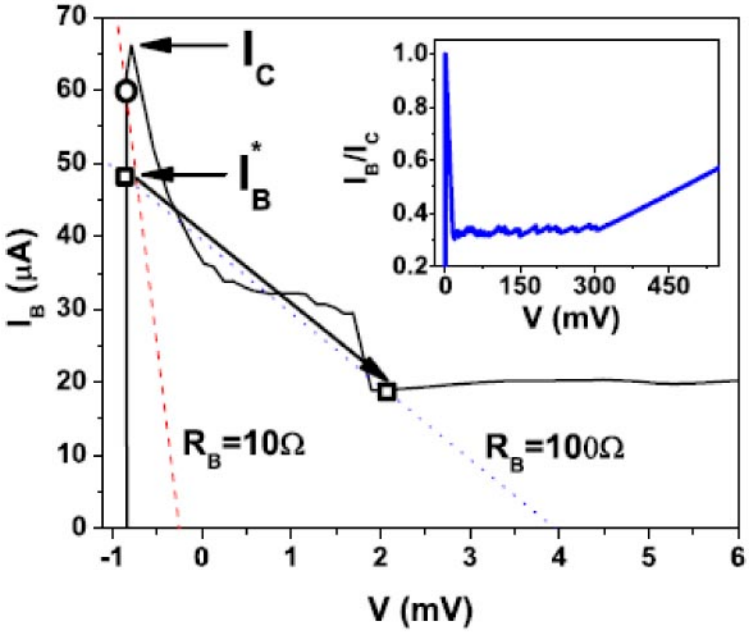

Fig. 3. I-V curve at 4.2K of a 100nm wide, 7nm thick meander (solid line) measured with R_B = 10Ω. For R_B = 10 Ω, the DC load line (dashed) never intersects the I-V both in the superconducting and hotspot plateau regions, which is not the case for higher values of R_B (dotted line, for R_B = 100 Ω). The voltage offset is due to thermoelectric effects (electrical contact from room temperature to the device is realized through junctions between different metals at different temperatures, so a voltage is created due to the Seebeck effect). The inset shows the I-V curve in a wider voltage range.

Source: Professor Francis Lévy, EPFL, Switzerland and Prof. Andrea Fiore, Photonics and Semiconductor Nanophysics Group, Dep. Applied Physics, Eindhoven University of Technology, contact person Prof. A. Fiore

Reference: F. Marsili, D. Bitauld, A. Fiore, A. Gaggero, F. Mattioli, R. Leoni, M. Benkahoul, and F. Lévy**,** "High efficiency NbN nanowire superconducting single photon detectors fabricated on MgO substrates from a low temperature process," Optics Express, Vol. 16, Issue 5, pp. 3191-3196 (**2008**)
http://dx.doi.org/10.1364/OE.16.003191

Thermal Electric Measurements Seebeck Effect

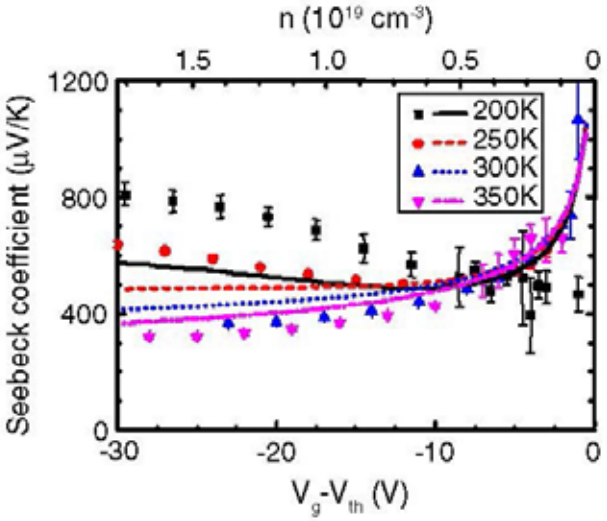

FIG. 2 (color online). Measurements (symbols) and calculations (lines) of the Seebeck coefficient vs gate bias in a pentacene thin film transistor. The gate bias Vg is corrected for the threshold voltage Vth of the TFT.

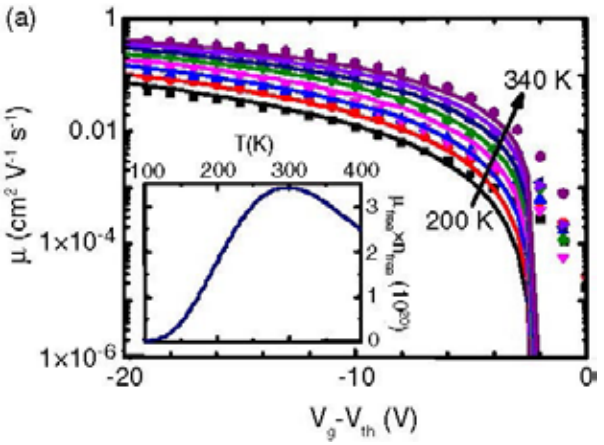

FIG. 3 (color online). (a) The measured (symbols) and calculated (lines) linear mobility vs gate bias with intervals of T = 20 K. The deviations at small gate voltage are attributed to leakage currents and the breakdown of the assumption that $|V_g - V_{th}| \gg V_{sd}$ = source-drain voltage). The inset shows $\mu_{free} \cdot n_{free} (\sim \sigma_{ME})$ vs T for $V_g - V_{th} = -30\ V$.

Source: Dr. Wijnand Germs, M.Sc., Molecular Materials and Nanosystems, Department of Applied Physics, University of Technology Eindhoven, The Netherlands

Reference: W. Chr. Germs, K. Guo, R. A. J. Janssen, and M. Kemerink, "Unusual Thermoelectric Behavior Indicating a Hopping to Bandlike Transport Transition in Pentacene," Phys. Rev. Lett. 109, 016601 (2012)
http://link.aps.org/doi/10.1103/PhysRevLett.109.016601

Metal Insulator Semiconductor Systems

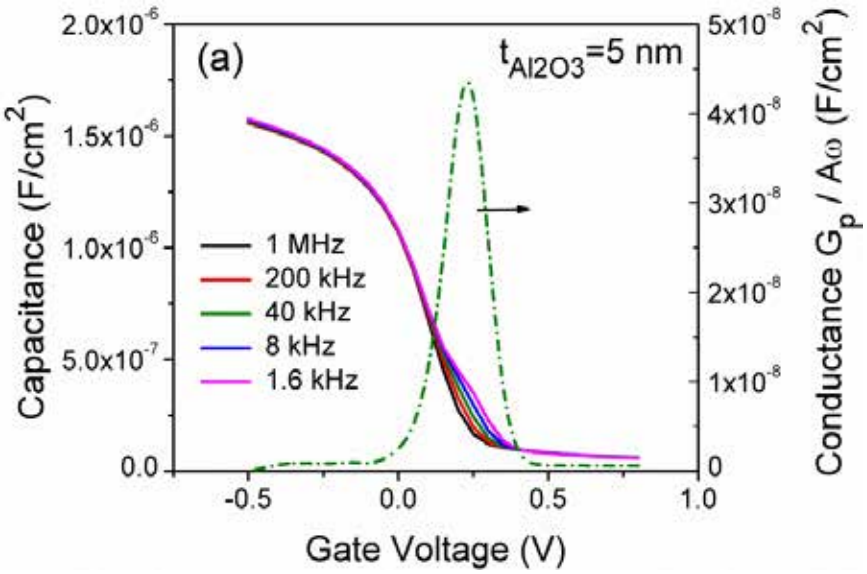

Fig.3. *C-V and G-V characteristics of Ge/Al2O3/Pt MIS structure measured at 80 K. Alumina thickness 5 nm.(unpublished).*

Source: Dr. Vassilios Ioannou-Sougleridis, Senior Researcher, Institute of Microelectronics, NCSR Demokritos

Reference: [1] P. Manousiadis, S. Gardelis, and A. G. Nassiopoulou, J. Appl. Phys. **109**, 083718 (2011).
[2] S. Gardelis, P. Manousiadis, and A. G. Nassiopoulou, Nanoscale Res. Lett. **6**, 227 (2011).
[3] D. Vellesiotis, A.M. Douvas, P. Dimitrakis, P. Argitis and N. Glezos, Microelectron. Eng. (2012) accepted for publication.
http://imel.demokritos.gr/index.shtml

Other Janis Cryostat Systems

He-3 refrigerator (270 mK)

Dilution refrigerator (8 mK)

Superconducting magnet systems

Other Janis Cryostat Systems

10 K and 4 K closed cycle refrigerator systems

Variable temperature LHe and/or LN_2 cooled cryostats

Custom engineered systems

Typical Applications and Materials

Applications

- MOS, MOSFET devices
- Solar cells
- Thermoelectrics
- Piezo-electrics
- Photodiodes
- Superconductivity
- MEMS, resonators and microsensors
- Quantum dots
- Nanowires and quantum wires
- Molecular electronics
- Magnetic recording devices
- LEDs
- Optics, optical communications
- IR detectors

Materials

- Graphene
- Carbon nanotubes
- Semiconductors
- Organic semiconductors
- Nanostructured semiconductors and semimetals
- Metals
- Insulators (dielectrics and ferroelectrics)
- Polymers
- Phase-change materials (chalcogenides)

Measurements

Properties

- Capacitance and conductivity measurements in the dark and under light.
- Capacitance-frequency; Capacitance-temperature
- C-V
- Electroluminescence
- Electromechanical and optical measurements with electrical actuation
- I(time)
- I-V
- Magnetoresistance
- Resistivity
- Photoconductivity
- Kelvin controller
- Light power vs current
- Photoluminescence
- Polarization-voltage
- Spectral response

Tools

- Semiconductor parameter (device) analyzer
- Impedance analyzer
- Network analyzers
- Pulse generator
- Source-Measurement-Unit

Acknowledgements

- Dr. Joshua Lee, Department of Electronic Engineering, City University of Hong Kong: www.ee.cityu.edu.hk/~joshulee
- Professor William Knowlton, Materials Science & Engineering | Electrical & Computer Engineering, Boise State University
- Dr. Richard L. McCreery, National Institute for Nanotechnology, University of Alberta, Canada
- Professor Yang Yang, University of California, Los Angeles, Department of Materials Science & Engineering. http://yylab.seas.ucla.edu/index.aspx
- Dr. Wijnand Germs, Molecular Materials and Nanosystems, Department of Applied Physics, University of Technology Eindhoven,
  The Netherlands
- Professor Eray Aydil, University of Minnesota
- Professor Eric Pop, Electrical and Computer Engineering, University of Illinois at Urbana-Champaign, http://poplab.ece.illinois.edu/publications.html, In particular journal papers #46, 39, 36, 34, 31, 30, 25 are all recent efforts that have utilized this Janis equipment. http://www.ece.illinois.edu/mediacenter/article.asp?id=371
- Professor Somnath Bhattacharyya , Nano-Scale Transport Physics Laboratory, School of Physics, University of the Witwatersrand, Johannesburg, South Africa,
- Francesco Pagliano and Andrea Fiore, Photonics and Semiconductor Nanophysics Group, Dep. Applied Physics, Eindhoven University of Technology, contact person Prof. A. Fiore
- Professor Eleanor Campbell and Dr. Johannes Svensson, formerly of Gothenburg University, Sweden and currently at Edinburgh University, UK and Lund University, Sweden respectively.
- Professor Francis Lévy, EPFL, Switzerland and Prof. Andrea Fiore, Photonics and Semiconductor Nanophysics Group, Dep. Applied Physics, Eindhoven University of Technology, contact person Professor A. Fiore
- Dr. Vassilios Ioannou-Sougleridis, Senior Researcher, Institute of Microelectronics, NCSR Demokritos

Papers Referenced

- Y. Xu and J. E.-Y. Lee, "Evidence on the impact of T-shaped tether variations on Q factor of bulk-mode square-plate resonator," in Proceedings of the 7th IEEE International Conference on Nano/Micro Engineered and Molecular Systems (IEEE NEMS 2012), Kyoto, Japan, 5-8 Mar 2012, pp. 463-468. http://dx.doi.org/10.1109/NEMS.2012.6196818
- Richard Southwick III*, J. Reed*, C. Buu*, H. Bui*, R. Butler*, G. Bersuker, and W.B. Knowlton, "Temperature (5.6-300K) Dependence Comparison of Carrier Transport Mechanisms in HfO_2/SiO_2 and SiO_2 MOS Gate Stacks," paper presentation at the 2008 IEEE International Integrated Reliability Workshop, (October 12-16, 2008), p.48-54. Invited to submit an extended version of this paper to IEEE Transactions on Materials and Device Reliability. http://dx.doi.org/10.1109/IRWS.2008.4796084
- Adam Bergren, Kenneth Harris, Fengjun Deng, and R. L. McCreery, "Molecular Electronics using Diazonium-Derived Adlayers on Carbon with Cu Top Contacts: Critical Analysis of Metal Oxides and Filaments", *J. Phys. Cond. Mat.* 2008, 20, 374117. (invited) http://iopscience.iop.org/0953-8984/20/37/374117/
- Jianyong Ouyang, Chih-Wei Chu, Charles R. Szmanda, Liping Ma, Yang Yang, "Programmable polymer thin film and non-volatile memory device," *Nature Materials, 3, 12, December (2004)* http://www.ncbi.nlm.nih.gov/pubmed/15568028
- Ankita Prakash, Jianyong Ouyang, Jen-Lien Lin, Yang Yang, "Polymer memory device based on conjugated polymer and gold nanoparticles," *Journal of Applied Physics, 100, 054309 (2006)* http://dx.doi.org/10.1063/1.2337252
- Erik M. Roeling, Wijnand Chr. Germs, Barry Smalbrugge, Erik Jan Geluk, Tjibbe de Vries, René A. J. Janssen & Martijn Kemerink, "Organic electronic ratchets doing work," *Nature Materials,* **10**, 51–55 (2011) doi:10.1038/nmat2922 www.nature.com/nmat/journal/v10/n1/full/nmat2922.html
- SeongHo Jeong, Sang Ho Song, Kushagra Nagaich, Stephen A. Campbell, Eray S. Aydil, "An analysis of temperature dependent current–voltage characteristics of Cu_2O–ZnO heterojunction solar cells," *Thin Solid Films*, Thin Solid Films 519, 6613-6619 (2011). http://dx.doi.org/10.1016/j.tsf.2011.04.241
- M.-H. Bae, Z.-Y. Ong, D. Estrada, E. Pop, "Imaging, Simulation, and Electrostatic Control of Power Dissipation in Graphene Devices," *Nano Letters* **10**, 4787, (2010). **Selected as cover article of *Nano Letters*, December 2010** http://dx.doi.org/10.1021/nl1011596
- Ross McIntosh, Messai A. Mamo, Brice Jamieson, Saibal Roy and Somnath Bhattacharyya, "Improved electronic and magnetic properties of reduced graphene oxide films," 2012 *EPL* **97** 38001, http://dx.doi.org/10.1209/0295-5075/97/38001. Ross McIntosh and Somnath Bhattacharyya, "The Kondo effect in reduced graphene oxide films," Phys. Status Solidi RRL **6**, No. 2, 56-58 (2012) / **DOI** 10.1002/pssr.201105493.
- Midolo et al., arxiv:1207.2980 (2012) http://arxiv.org/abs/1207.2980
- Kurtis S. Leschkies, Moon Sung Kang, Eray S. Aydil and David J. Norris, "Influence of Atmospheric Gases on the Electrical Properties of PbSe Quantum-Dot Films," *J. Phys. Chem. C*, **2010**, *114* (21), pp 9988–9996 http://pubs.acs.org/doi/abs/10.1021/jp101695s
- Svensson J, Sourab AA, Tarakanov Y, Lee DS, Park SJ, Baek SJ, Park YW, Campbell EE, "The dependence of the Schottky barrier height on carbon nanotube diameter for Pd-carbon nanotube contacts.;" Nanotechnology. 2009 Apr 29;20(17):175204. http://www.ncbi.nlm.nih.gov/pubmed/19420588 and http://nanotechweb.org/cws/article/tech/39382.
- F. Marsili, D. Bitauld, A. Fiore, A. Gaggero, F. Mattioli, R. Leoni, M. Benkahoul, and F. Lévy**,** "High efficiency NbN nanowire superconducting single photon detectors fabricated on MgO substrates from a low temperature process," Optics Express, Vol. 16, Issue 5, pp. 3191-3196 (**2008**) http://dx.doi.org/10.1364/OE.16.003191
- W. Chr. Germs, K. Guo, R. A. J. Janssen, and M. Kemerink, "Unusual Thermoelectric Behavior Indicating a Hopping to Bandlike Transport Transition in Pentacene," Phys. Rev. Lett. 109, 016601 (2012) http://link.aps.org/doi/10.1103/PhysRevLett.109.016601
- [1] P. Manousiadis, S. Gardelis, and A. G. Nassiopoulou, J. Appl. Phys. **109**, 083718 (2011).
  [2] S. Gardelis, P. Manousiadis, and A. G. Nassiopoulou, Nanoscale Res. Lett. **6**, 227 (2011).
  [3] D. Vellesiotis, A.M. Douvas, P. Dimitrakis, P. Argitis and N. Glezos, Microelectron. Eng. (2012) accepted for publication.
  http://imel.demokritos.gr/index.shtml

Other Customer Papers

- Mattias Andersson, Linkoping University, Sweden,
  Organic Electronics 12 (2011) 300–305
  Organic Electronics 9 (2008) 569–574

- Chris Papadopoulos, University of Victoria, Canada
  C. Papadopoulos, et al. IEEE Transactions on Nanotechnology, May 2010, Volume: 9, Issue: 3, Pages 375-380, "A Direct-Write Approach for Carbon Nanotube Catalyst Deposition" http://dx.doi.org/10.1109/TNANO.2009.2029856

- Boon S. Ooi, King Abdullah University of Science and Technology (KAUST), Saudi Arabia
  www.kaust.edu.sa

- Dr Jo Shien Ng, Royal Society University Research Fellow/Senior Lecturer Elect, Department of Electronic & Electrical Engineering, The University of Sheffield, United Kingdom, D S G Ong, J S Ng, Y L Goh, C H Tan, S Zhang, and J P R David, "InAlAs avalanche photodiode with type-II superlattice absorber for detection beyond 2 micron," *IEEE Trans. Electron Devices*, 58(2), pp. 486-489, Feb 2011. Figure 2.
  http://impact-ionisation.group.shef.ac.uk/

- Dr. Nurit Ashkenasy, Department of Materials Engineering, Ben Gurion University of the Negev, Israel, Research interests: bioelectronics
  "We are using the probe station to measure the electronic properties of nanostructures based on peptidic materials. Our system is equipped with 3 conventional probes and one probe that is able of measuring the work function of the samples (a kelvin probe). The instrument allows us to measure the electronic properties in air, vacuum, as function of humidity and as function of the temperature. A monochromator that will be coupled to the system within the next couple of weeks will allow us to measure the photoelectric response of our sample. This system has been used to study structure function relation in fibrils based on a sequence from the b-amyloid protein. Indeed, we were able to show that the conductance depends greatly on both the chemical and morphological structure. We have also observed an exponential dependence on the humidity, the origin of which we are currently investigating."
  http://www.bgu.ac.il/~nurita/

- Jeremie Grisolia, LPCNO INSA-Departement de Pysique, France
  www.alma-conseil.com/lpcno

- Prof. D. Tsoukalas, National Technical University of Athens, Greece
  J.L. Tanner, D. Mousadakos, K. Giannakopoulos, E. Skotadis, and D. Tsoukalas, "High strain sensitivity controlled by the surface density of platinum nanoparticles," Nanotechnology 23 (2012) 285501 (6pp) http://dx.doi.org/10.1088/0957-4484/23/28/285501
  Nanoparticle film senses strain with high sensitivity, http://nanotechweb.org/cws/article/lab/50231

- Behraad Bahreyni, Simon Fraser University, Canada
  "We have two vacuum probe stations from Janis that we use for testing Silicon chips as well as packaged devices. The probe stations are hooked up to network analyzers for most applications and are often used to test micromachined resonators." Pictures and results at http://imuts.ensc.sfu.ca

- Bernard Plaçais, Head of the network "Physique Quantique Mésoscopique" (CNRS, GDR-242 6), Head of the Mesoscopic Physics Group, Laboratoire Pierre Aigrain (ENS)
  http://www.phys.ens.fr/~placais/

- Dr W. Favre, Post-doc (CEA-INES, France)
  http://www.ines-solaire.org/

- Jérémie GRISOLIA, Assistant Professor, Université de Toulouse, INSA-CNRS-UPS, LPCNO, France
  "Extraction of the characteristics of Si nanocrystals by the charge pumping technique"
  R Diaz, J Grisolia, G BenAssayag, S Schamm-Chardon, C Castro, B Pecassou, P Dimitrakis and P Normand. Nanotechnology 23 (2012) 085206.
  "Tunable Conductive Nanoparticle Wire Arrays Fabricated by Convective Self-Assembly on Nonpatterned Substrates" Cosmin Farcau, Helena Moreira, Benoît Viallet, Jérémie Grisolia, and Laurence Ressier* ***ACS Nano***, 2010, 4 (12), pp 7275–7282 ***(2010)***

- Dr. Ali Gokirmak, Assistant Professor, ECE, University of Connecticut
  http://www.engr.uconn.edu/electron/index.html

- Dr. Seth M. Hubbard, Associate Professor of Physics and Microsystems Engineering, Graduate Faculty Golisano Institute for Sustainability, Rochester Institute of Technology, "Thermal and Spectroscopic Characterization of Quantum Dot-Enhanced Solar Cells"
  http://www.sustainability.rit.edu/nanopower

For more Information

Contact Janis Research at

sales@janis.com

www.janis.com/ProbeStations.aspx